Effect of the environment on star formation activity and stellar mass for star-forming galaxies in the COSMOS field

S. M. Randriamampandry,[1,2]★ M. Vaccari [ORCID][3,4] and K. M. Hess[5,6]

[1]*South African Astronomical Observatory, PO Box 9, Observatory 7935, Cape Town, South Africa*
[2]*A&A, Department of Physics, Faculty of Sciences, University of Antananarivo, B.P. 906, Antananarivo 101, Madagascar*
[3]*Department of Physics and Astronomy, University of the Western Cape, Robert Sobukwe Road, Bellville 7535, South Africa*
[4]*INAF - Istituto di Radioastronomia, via Gobetti 101, I-40129 Bologna, Italy*
[5]*ASTRON, the Netherlands Institute for Radio Astronomy, PO Box 2, 7990 AA Dwingeloo, the Netherlands*
[6]*Kapteyn Astronomical Institute, University of Groningen, PO Box 800, 9700 AV Groningen, the Netherlands*

ABSTRACT

We investigate the relationship between the environment and the galaxy main sequence (the relationship between stellar mass and star formation rate), as well as the relationship between the environment and radio luminosity ($P_{1.4\,GHz}$), to shed new light on the effects of the environment on galaxies. We use the VLA-COSMOS 3-GHz catalogue, which consists of star-forming galaxies and quiescent galaxies (active galactic nuclei) in three different environments (field, filament, cluster) and for three different galaxy types (satellite, central, isolated). We perform for the first time a comparative analysis of the distribution of star-forming galaxies with respect to the main-sequence consensus region from the literature, taking into account galaxy environment and using radio observations at $0.1 \leq z \leq 1.2$. Our results corroborate that the star formation rate is declining with cosmic time, which is consistent with the literature. We find that the slope of the main sequence for different z and M_* bins is shallower than the main-sequence consensus, with a gradual evolution towards higher redshift bins, irrespective of environment. We see no trends for star formation rate in either environment or galaxy type, given the large errors. In addition, we note that the environment does not seem to be the cause of the flattening of the main sequence at high stellar masses for our sample.

Key words: galaxies: evolution – galaxies: star formation – galaxies: stellar content.

1 INTRODUCTION

Star formation is one of the principle indicators of the evolution of galaxies, and it can be used as one of the main tracers of galaxy evolution. It allows us to characterize the newly born stars in the galaxy by measuring the star formation rate (SFR), which is the total mass of stars formed per year. Furthermore, star formation history (SFH) is important as it enables us to find changes in the SFR across cosmic time, and hence it traces the evolution of the galaxy. An estimate of the integrated SFH of a galaxy can be inferred from stellar mass (see Brinchmann & Ellis 2000; Heavens et al. 2004; Treu et al. 2005) via the relationship between star formation and the growth of stellar mass; it is defined as specific SFR (sSFR = SFR/M_*, i.e. the star formation rate per unit stellar mass).

Star formation activity further correlates strongly with galaxy stellar mass (M_*). This relationship was analysed for the first time by Noeske et al. (2007), who called it the star formation main sequence (MS), and it has been extensively studied ever since (see Daddi et al. 2007; Pannella et al. 2009; Magdis et al. 2010; Rodighiero et al. 2011; Whitaker et al. 2012; Stark et al. 2013; Steinhardt et al. 2014; Ilbert et al. 2015; Barro et al. 2017; Pearson et al. 2018; Popesso et al. 2019). Star-forming galaxies (SFGs) along the MS relation have star

formation self-regulated by secular processes and at a level dictated predominantly by their stellar masses (e.g. Whitaker et al. 2014; Leja et al. 2015). The MS relation implies that SFHs over an averaged population of SFGs are mostly regular, smooth and deceasing with an M_*-dependent time-scale (e.g. Heavens et al. 2004) prior to the shutdown of star formation.

The universality of the observed MS relation for SFGs has been investigated for over a decade and has been found to hold for a wide range of redshift from the local Universe at $z \simeq 0$ (see Brinchmann et al. 2004; Salim et al. 2007), to $z \simeq 1$ (e.g. Elbaz et al. 2007; Noeske et al. 2007; Ilbert et al. 2015), $z \simeq 2$ (see Daddi et al. 2007; Pannella et al. 2009; Rodighiero et al. 2011; Whitaker et al. 2012; Kochiashvili et al. 2015), and from $z \simeq 3$ (e.g. Magdis et al. 2010; Barro et al. 2017) to $z \simeq 4$ (e.g. Daddi et al. 2009; Pannella et al. 2015), and even up to higher than $z \sim 7$ (see Bouwens et al. 2012; Stark et al. 2013; Steinhardt et al. 2014; Salmon et al. 2015). Furthermore, there are MS studies that have already been conducted at $0.2 \leq z < 6$ with the far-infrared *Herschel* Spectral and Photometric Imaging Receiver (SPIRE; e.g. Pearson et al. 2018). So, the relationship has been in place for at least 90 per cent of the age of the Universe. Therefore, it can be used to characterize how instantaneous star formation is determined by the past SFHs of an individual SFG or a subset of the population of SFGs.

However, other studies suggest that the SFR in SFGs can be regulated and quenched by different physical processes linked to

★ E-mail: solohery@saao.ac.za

environments such as galaxy interactions and galaxy minor/mergers (e.g. Peng et al. 2010; Guo, Zheng & Fu 2013; Contini et al. 2020), which may alter the properties of the MS relation. Despite these processes, and despite the different methods used to measure the galaxy properties, the MS relation still holds. Furthermore, its characteristics have been reproduced in numerical simulations up to at least $z \sim 3$ (e.g. Finlator et al. 2006; Davé et al. 2010; Davé, Oppenheimer & Finlator 2011; Tacchella et al. 2016). Previous studies that have looked at the MS of SFGs in different environments have found that cluster galaxies and those found in groups have lower sSFR compared with field galaxies (e.g. Vulcani et al. 2010; Haines et al. 2013; Lin et al. 2014; Jian et al. 2017). The cluster, the field and the filament environments of galaxies shape their properties, such as colour and mass, thus playing important roles in their evolution over cosmic time (e.g. Baldry et al. 2006; Muzzin et al. 2012; Jian et al. 2018) and hence in their ultimate fate.

In this work, we targeted a large population of SFGs at $0.1 < z < 1.2$ from one of the deepest radio surveys publicly available with a 'clean' separation of SFGs from active galactic nuclei (AGNs). We used 1.4-GHz luminosity, which traces the synchrotron emission from SFGs. The non-thermal radio luminosity can be an excellent dust-free estimator of star formation (see Condon 1992; Bell 2003; Murphy et al. 2011) so, in addition, we attempt to use it to look at the behaviour of the radio luminosities of our larger radio-selected sample of SFGs across different environments. The investigation of the MS relation as well as the radio luminosity of SFGs as a function of the environment and galaxy type may clarify the role of environmental processes in galaxy evolution. We aim to study the relationship between the SFR and stellar mass M_* of SFGs, and also the relationship between environment and radio luminosity ($P_{1.4\,\mathrm{GHz}}$), to shed new light on the effects of the environment (field, filament, cluster) on various galaxy types (satellites, central, isolated) at $0.1 \leq z \leq 1.2$. To the best of our knowledge, no other work has looked at the MS by taking advantage of one of the deepest available radio surveys. By considering multiwavelength data for these galaxies and the available measurements of their environments, we have been able to investigate the effect of the environment on the galaxy MS in a unique way.

The paper is organized as follows. In Section 2, we present our sample of SFGs and their properties, and we present our results in Section 3. In Sections 4 and 5, we discuss and summarize our findings, and suggest some future work. Throughout this paper, we adopt $H_0 = 71$ km s^{-1} Mpc^{-1}, $\Omega_m = 0.27$ and $\Omega_{DE} = 0.73$.

2 SAMPLE AND GALAXY PROPERTIES

For our analysis, we take advantage of data from the Cosmic Evolution Survey (COSMOS;[1] Scoville et al. 2007) field in the available redshift range of $0.1 \leq z \leq 1.2$. The COSMOS is a multiwavelength survey that covers a field of view of 2 deg^2, and is centred at RA $= +150.119167$ and Dec. $= +2.205833$. The survey aims to study galaxy formation and evolution as a function of redshift, out to $z \sim 5$, and the large-scale structure environment. The details of COSMOS and its observations are described in Scoville et al. (2007). In the following subsections, we provide a description of our sample and its properties, and also we indicate where they particularly come from.

Table 1. The breakdown of the total number of galaxies for each cosmic web environment (field, filament, cluster) and for each galaxy type (satellite, central, isolated) in our sample.

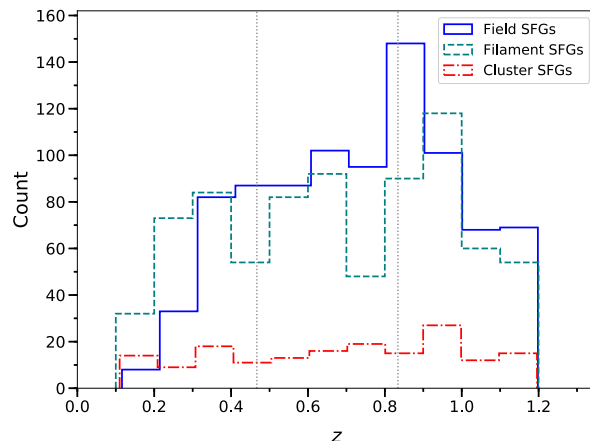| Field	Filament	Cluster	Satellite	Central	Isolated
880	787	169	697	450	689

Figure 1. Histogram of the redshifts of our sample. The three different environment estimators from Darvish et al. (2017) are shown as the blue solid line for field, cyan dashed line for filament and red dash-dotted line for cluster SFGs. The grey dotted lines indicate the bin width of each subsample that we use throughout the paper. (A colour version of this figure is available in the online journal.)

2.1 Sample

In this work, we used a sample of radio-selected SFGs drawn from the multiwavelength catalogue[2] compiled by Smolčić et al. (2017b), which is based on the Very Large Array (VLA) COSMOS 3-GHz Large Project radio source catalogue (Smolčić et al. 2017a). To form our sample, we complemented the Smolčić et al. (2017b) catalogue with two ancillary catalogues: the cosmic web environment[3] catalogue of Darvish et al. (2015, 2017) for studying the effects of the environment (field, filament, cluster) on the star formation MS for various type of galaxies (satellite, central, isolated), and a photometric catalogue from the COSMOS survey conducted in 2015 (COSMOS2015;[4] Laigle et al. 2016) to obtain stellar mass M_* and photometric redshift z for each galaxy. We did all the matching using COSMOS2015 source identification numbers.

The final number of sources from these matching procedures resulted in 2568 radio detections with counterparts in the other catalogues (note that we eliminate 'bad data' that have FLAG $= 1$ in the COSMOS2015 catalogue), where 1836 are SFGs and 732 are AGNs. Smolčić et al. (2017b) used observations based on X-rays, mid-infrared and spectral energy distributions to separate AGNs/SFGs plus a combined rest-frame colour and radio excess diagnostic to obtain a 'clean' sample of SFGs. We removed those AGNs from our sample, so we focus on only the SFGs in the rest of the paper.

Table 1 summarizes the number of galaxies by their respective environments and galaxy types. Fig. 1 shows the redshift distribution

---

[1] http://cosmos.astro.caltech.edu/page/astronomers

[2] http://jvla-cosmos.phy.hr/dr1/
[3] https://irsa.ipac.caltech.edu/data/COSMOS/tables/environment/
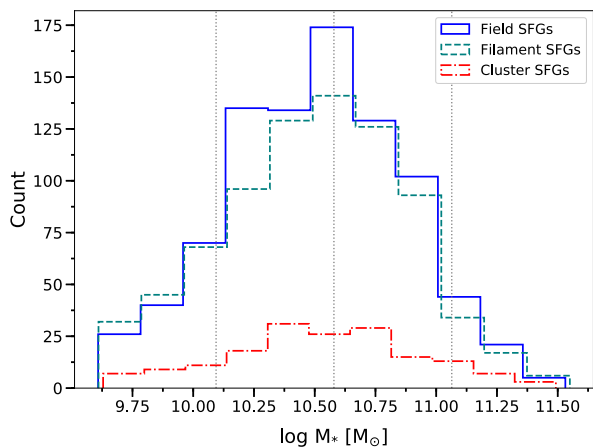[4] ftp://ftp.iap.fr/pub/from_users/hjmcc/COSMOS2015/

Figure 2. Histogram of stellar masses of our sample. The three different environment estimators from Darvish et al. (2017) are shown as the blue solid line for field, cyan dashed line for filament and red dash-dotted line for cluster SFGs. The grey dotted lines indicate the bin width of each subsample that we use throughout the paper. (A colour version of this figure is available in the online journal.)

of our sample where the three different environment estimators from Darvish et al. (2017) are indicated.

2.2 Properties of galaxies

We use the derived M_* from the COSMOS2015 catalogue, which are based on SED-fitting using the Stellar Population Synthesis (SPS) model of Bruzual & Charlot (2003) (BC03) templates by assuming an initial mass function (IMF) of Chabrier (2003). The full details of the method for estimating M_* are presented in Ilbert et al. (2015) and Laigle et al. (2016). We show the histogram of M_* in Fig. 2 where the three different environment estimators from Darvish et al. (2017) are indicated as in Fig. 1. We note that the M_* normalized distributions are similar across the different environments.

The SFRs were measured by Smolčić et al. (2017b), and estimated from the total infrared luminosity using the Kennicutt (1998b) conversion factor scaled to a Chabrier (2003) IMF. In addition, the rest-frame 1.4-GHz radio luminosity was measured from the 1.4–3 GHz spectral index, when available, or assuming a spectral index[5] of $\alpha = 0.7$. Fig. 3 shows the distribution of 1.4-GHz radio luminosity ($P_{1.4\,GHz}$) of our sample. The full details of the method for measuring the total infrared luminosity, SFRs and $P_{1.4\,GHz}$ are presented in Smolčić et al. (2017b).

Finally, the measurements of local environments are based on a density field constructed using the weighted adaptive kernel smoothing estimator (Darvish et al. 2015, 2017). The components of the cosmic web environments (filament, cluster and field) are then extracted from the constructed density field through the Hessian matrix technique (see Darvish et al. 2017). The classification of galaxy type (central, satellite and isolated) is observationally identified through galaxy groups, where the most massive galaxy in each single group is selected as a central galaxy and the rest as satellites, or otherwise isolated if not associated with any groups. Groups of galaxies are identified using the commonly used friends-of-friends

---

[5]Note that α is the power-law slope of the synchrotron radiation, and is defined as $S_\nu \sim \nu^{-\alpha}$, where S_ν and ν are the flux density and frequency, respectively.
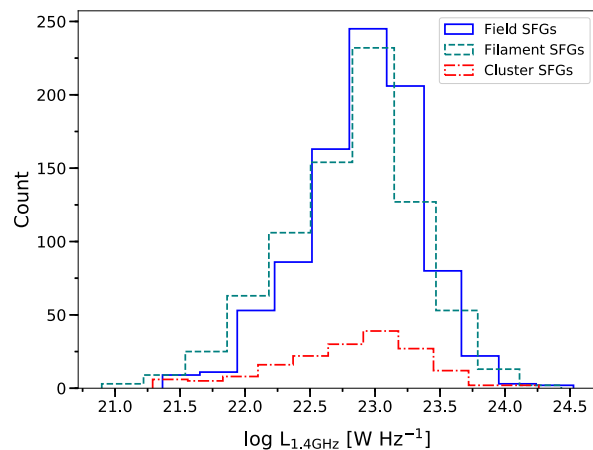
Figure 3. Histogram of radio luminosities for our sample. The three different environment estimators from Darvish et al. (2017) are shown as the blue solid line for field, cyan dashed line for filament and red dash-dotted line for cluster SFGs. (A colour version of this figure is available in the online journal.)

algorithm (Huchra & Geller 1982; Duarte & Mamon 2014; Darvish et al. 2017). We refer the reader to Darvish et al. (2015, 2017) for full details on the cosmic web measurements and the classification of galaxy types.

3 RESULTS

3.1 Main sequence of SFGs and environments

3.1.1 Aim and approach

Our primary aim is to look at the differences of the MS of SFGs with respect to environment as a function of redshift. To do so, we compare our results to the MS consensus of Speagle et al. (2014), who collated and calibrated 25 MS studies of SFGs, taken from a range of multiwavelength observations (ultraviolet to radio) in the literature. Their MS consensus at ±0.2 dex dispersion was compiled based on the M_* and SFR measured using the BC03 SPS model with the Kroupa IMF (Speagle et al. 2014). We choose their MS consensus as a benchmark to which we compare our work, because the galaxy properties of our sample were measured with the same SPS model. The chosen MS consensus enables us to minimize some systematics due to sample selection effects, SFR indicators and methods used to locate the MS when comparing different results from the literature.

Our results, such as M_*, were measured via SED fitting through the χ^2 method based on best-fitting templates using optical/near-infrared photometry and the BC03 SPS model specifically using a Chabrier IMF. For conformity in the comparison, we convert M_*, SFR and the MS consensus and any other MS from the literature into the Chabrier IMF. We use a conversion for the IMF for both M_* and SFR by following equation (2) of Speagle et al. (2014), which is defined as Kroupa = $1.06 \times$ Chabrier = $0.62 \times$ Salpeter. We adapt this relation for M_* and SFR by assuming that these have similar relative offsets. A similar ratio has been observed for the SFR via a conversion from the Salpeter SFR (Kennicutt 1998a) to the Kroupa SFR (Kennicutt & Evans 2012). We also use SFR in this work instead of sSFR for direct comparison to the control sample from Speagle et al. (2014). Throughout the paper, we take into account this conversion when comparing M_* and SFR from any other studies.

To disentangle any redshift and/or M_* dependence on the MS for a given environment, we have divided our sample of SFGs into three

Table 2. The breakdown of the total number of galaxies for each z and M_* bin.

z and M∗ bins	Number of sources
First ($0.10 \leq z < 0.47$)	435
Second ($0.47 \leq z < 0.83$)	697
Third ($0.83 \leq z \leq 1.20$)	704
First ($9.6 \leq \log M_* < 10.1$)	275
Second ($10.1 \leq \log M_* < 10.6$)	812
Third ($10.6 \leq \log M_* < 11.1$)	647
Fourth ($11.1 \leq \log M_* < 11.6$)	102

bins of equal width, such that the first bin is at $0.10 \leq z < 0.47$, the second bin is at $0.47 \leq z < 0.83$ and the third bin is at $0.83 \leq z \leq 1.20$. Likewise, we split sources into four M_* bins with a width of approximately 0.5 dex such that the first bin is for $9.6 \leq \log M_* < 10.1$, the second bin is for $10.1 \leq \log M_* < 10.6$, the third bin is for $10.6 \leq \log M_* < 11.1$ and the last bin is for $11.1 \leq \log M_* < 11.6$.

Throughout the work, we refer to these bins as the lower, intermediate and higher redshift or M_* bins, respectively. Table 2 presents the total number of galaxies for each z and M_* bin. We note that although these bins have similar widths, when interpreting our results we strive to take into account the number of sources in each bin in order to minimize bias.

To disentangle the completeness limit, in a similar way to Bonzini et al. (2015, see fig. 5), we use the empirical relationship between radio luminosity and SFR of Delhaize et al. (2017) to estimate the SFR limits. Using the minimum $P_{1.4\,\mathrm{GHz}}$ in each single redshift bin, the SFR limit is defined as

$$\mathrm{SFR}\ (\mathrm{M_\odot\ yr^{-1}}) = f_{\mathrm{IMF}}10^{-24}10^{q_{\mathrm{TIR}}(z,\alpha)} \times P_{1.4\,\mathrm{GHz}}\ (\mathrm{W\,Hz^{-1}}),$$

where

$$q_{\mathrm{TIR}}(z) = \begin{cases} (2.88 \pm 0.03)(1+z)^{-0.19\pm0.01} & \text{for } \alpha = 0.7 \\ (2.85 \pm 0.03)(1+z)^{-0.22\pm0.01} & \text{for } \alpha = 0.8 \end{cases},$$

and f_{IMF} is a factor accounting for the assumed initial mass function ($f_{\mathrm{IMF}} = 1$ for a Chabrier IMF). Note that $q_{\mathrm{TIR}}(z,\alpha)$ is the infrared-to-1.4-GHz radio luminosity ratio where z and α are the average redshift in each bin and the average assumed spectral index of the SFG population, respectively.

The relationship between the SFR and the stellar mass of SFGs for the three different environments is shown in Fig. 4. The black solid line in each panel indicates the best-fitting MS consensus of Speagle et al. (2014) at $z = 0.25$ (top), $z = 0.5$ (middle) and $z = 1$ (bottom), while the shaded yellow region indicates a scatter of ±0.2 dex consensus dispersion. The black dash-dotted lines indicate the MS consensus of Speagle et al. (2014) at $z = 0$ and 0.5 (top), $z = 0.25$ and 1 (middle) and $z = 0.5$ and 2 (bottom), respectively, which are shown as a benchmark for comparison.

In the left-hand panels of Fig. 4, the black dotted (and triangle down) horizontal lines indicate the estimated SFR limits. In each right-hand panel of Fig. 4, we plot the mean of the SFR (which agrees with the median within ≈0.2 dex) and the errors shown are based on the standard error of the mean. We additionally compare our results to the best-fitting MS lines from Whitaker et al. (2012) in order to further quantify the slopes of our data as also shown in Fig. 4 (right-hand panels). For conformity in the comparisons, we choose to further compare to the MS from Whitaker et al. (2012) as it is similar to the MS consensus of Speagle et al. (2014).

3.1.2 Results of MS of SFGs

In Fig. 4, we plot the MS of our binned sample where each row represents a different redshift bin. The left column presents the individual data points coloured by galaxy environments and the right column presents the mean trends of each environment, binned by galaxy stellar mass. The slopes and intercepts from our best-fitting lines are shown in Table 3.

The top-left panel of Fig. 4 shows that most of our sources are above the MS consensus in this lower redshift bin ($0.10 \leq z < 0.47$) regardless of the environment. These galaxies located at the upper envelope of the MS consensus are actively forming stars (i.e. sources that are further up from the yellow region). They seem to be observed to fit better to the benchmark MS consensus line at $z = 0.5$ across the M_* range. In addition, we find that the slope of our best fit shown by the dashed line, irrespective of environment at $0.10 \leq z < 0.47$, seems to be shallower than the MS consensus.

We also see that one of the cluster SFGs and one field SFGs at $0.47 \leq z < 0.83$ (middle-left panel) are below the estimated SFR limits shown by the dotted horizontal lines. Furthermore, we see that quite a few of the sources are below the estimated SFR limit at $0.83 \leq z \leq 1.20$ (bottom-left panel). These radio sources detected under SFR limits, regardless of their environment, observed at the highest redshift bin, appear to be associated with the spectral index as the two lines seem to depend on the assumed spectral index (i.e. $\alpha = 0.7$ and 0.8) as well as cosmic time. The sensitivity limits deepen as the spectral index steepens when redshift increases. See also Section 3.3 for further discussion of SFR limits.

The top-right panel of Fig. 4 examines the behaviour of the MS as a function of the average M_* for four M_* bins. The slope of the MS for each respective environment appears to be shallower when compared with both the MS consensus and the best fit of Whitaker et al. (2012) at a similar redshift bin ($0 < z < 0.5$). For cluster SFGs, regardless of the flat slope towards the highest z bin, we may find better agreement between our MS and the MS consensus. Nevertheless, both the field and filament SFGs do not agree with the yellow region at lower M_* bins ($9.6 \leq \log M_* < 10.1$ and $10.1 \leq \log M_* < 10.6$).

In the middle panels of Fig. 4, we show the MS for the intermediate redshift bin ($0.47 \leq z < 0.83$). The middle-left panel of Fig. 4 shows that there are still sources above the MS consensus, regardless of the environment, where most sources are above the consensus dispersion region (shaded yellow) across the M_* range. We observe that the slope of our best fit shown by the dashed line may also be even shallower than the MS consensus in this bin at $0.47 \leq z < 0.83$.

In the middle-right panel of Fig. 4, we notice that the average SFR for the lowest bin is above the MS consensus benchmark line and could be due to averaging a lower number of sources in this bin. The slope of the MS for each respective environment may also be even shallower when compared with both the MS consensus and the best fit of Whitaker et al. (2012) at a similar redshift bin ($0.5 < z < 1$). The best-fitting line from Whitaker et al. (2012) and the MS consensus line have the same slope and are in agreement within the consensus dispersion. We also find that the mean SFRs for all sources do not agree with the yellow region at lower M_* bins ($9.6 \leq \log M_* < 10.1$ and $10.1 \leq \log M_* < 10.6$).

In the bottom panels of Fig. 4, we present the MS for the highest redshift bin ($0.83 \leq z \leq 1.20$). The bottom-left panel of Fig. 4 shows that, regardless of the environment, our sources appear to be clustered around the MS consensus and a higher fraction of them seem to be located in the MS consensus region shaded yellow. We find that the slope of our best fit shown by the dashed line may even be more shallow than the MS consensus. The bottom-right panel of Fig. 4
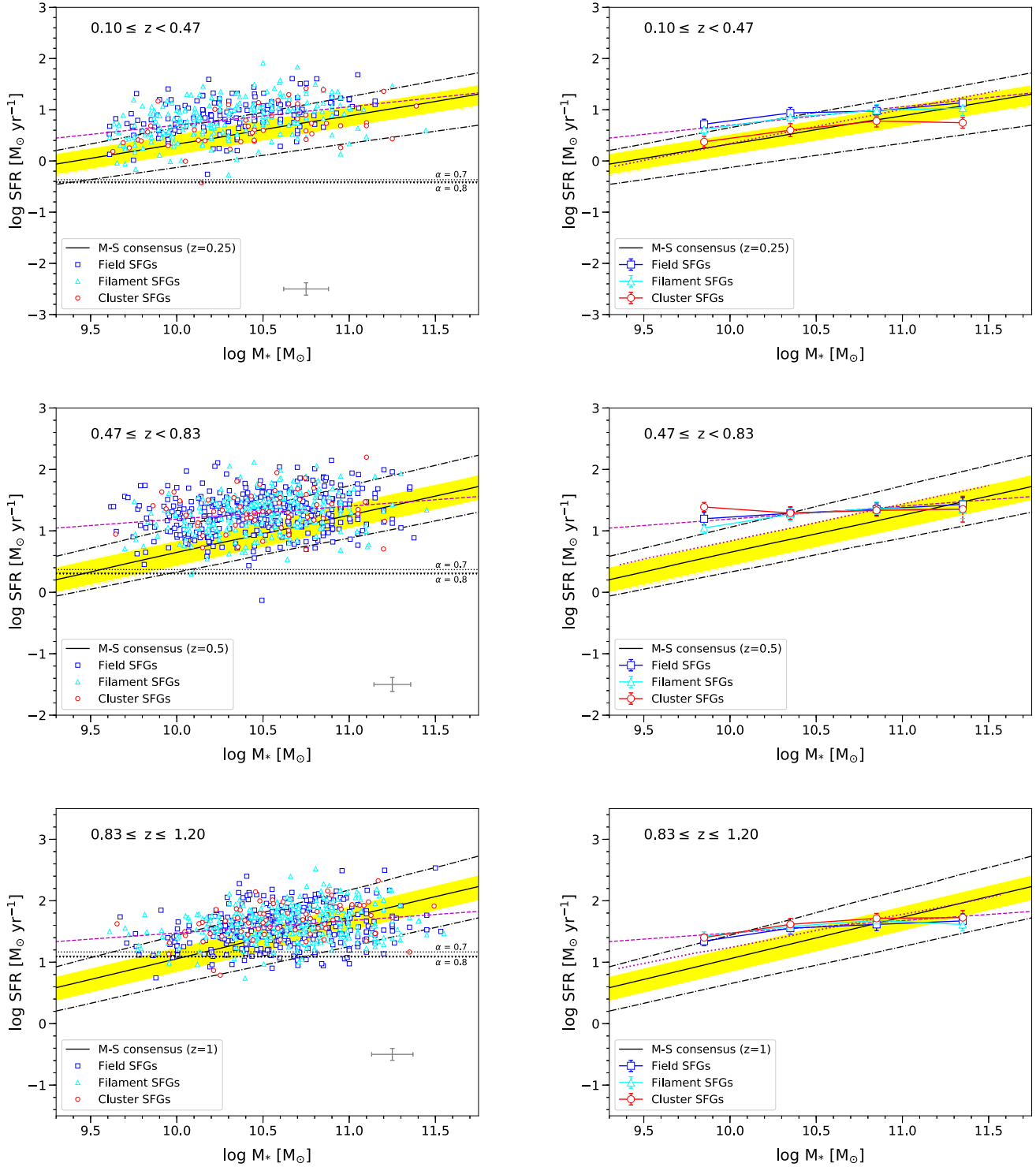
Figure 4. SFR versus stellar mass M_* of SFGs for the three different environments for the lower (top), intermediate (middle) and higher (bottom) z bins. In each panel, the blue squares, teal triangles and red circles represent field, filament and cluster SFGs, respectively. The black solid lines indicate the MS consensus of Speagle et al. (2014) at $z = 0.25$ (top), $z = 0.5$ (middle) and $z = 1$ (bottom) while the shaded yellow region indicates a scatter of ±0.2 dex consensus dispersion. The black dash-dotted lines indicate the MS consensus of Speagle et al. (2014) at $z = 0$ and 0.5 (top), $z = 0.25$ and 1 (middle) and $z = 0.5$ and 2 (bottom), respectively, which are shown as a benchmark for comparison. The magenta dashed lines shows the best fit to the entire population of source (irrespective of environment). The left-hand panels show the scatter plots of the SFGs upon the MS consensus. The black dotted (for $\alpha = 0.7$) and triangle down (for $\alpha = 0.8$) horizontal lines indicate the estimated SFR limits calculated for each redshift bin, based on the SFR and radio luminosity model of Delhaize et al. (2017). The grey solid cross lines in the bottom-right corners represent the error bars, which correspond to average 1σ errors based on the standard error of the mean. The right-hand panels present the behaviour of the average M_* of the four M_* bins for the three environments. For further comparison, the best-fitting MS from Whitaker et al. (2012) for each similar z bin is also shown by the magenta dotted line. (A colour version of this figure is available in the online journal.)

Table 3. Summary of the calculated slopes and intercepts for each z bin.

z bin	Slope	Intercept
First ($0.10 \leq z < 0.47$)	0.360 ± 0.042	2.899 ± 0.431
Second ($0.47 \leq z < 0.83$)	0.210 ± 0.034	0.905 ± 0.359
Third ($0.83 \leq z \leq 1.20$)	0.201 ± 0.031	0.530 ± 0.325

shows that the slope of the MS for each respective environment may also be even more shallow when compared with both the MS consensus and the best fit of Whitaker et al. (2012) at a similar redshift bin ($1 < z < 1.5$). We observe that the mean SFRs for all sources do not agree with the yellow shaded region at most M_* bins ($9.6 \leq \log M_* < 10.1$, $10.1 \leq \log M_* < 10.6$ and $11.1 \leq \log M_* < 11.6$).

In the left-hand panels of Fig. 4, overall we might detect larger numbers of MS galaxies with lower stellar mass ($\log M_* < 10$) in the first two redshift bins ($0.10 \leq z < 0.47$ and $0.47 \leq z < 0.83$) where the best fit for the MS seem to be the upper benchmark lines at $z = 0.5$ and 1, respectively. However, at a higher redshift bin ($0.83 \leq z \leq 1.20$) we might probe the bulk of the MS galaxies mostly at the high-mass end ($\log M_* < 10$) where the best-fitting consensus ($z = 1$) fits the MS galaxies well.

3.2 Environment versus galaxy type

In Fig. 5, we present the average log SFR of our (both z and M_*) binned sample where the top row represents the three different environments (field, filament, cluster) and the bottom row represents the three different galaxy types (satellite, central, isolated). We note that in the non-scaled x-axis in Fig. 5 (and likewise in Fig. 6) we have plotted from the less-dense to more-dense category, both for the environment and for the galaxy type, with the aim of tracing any trend in the distribution of galaxies for the different categories as we move from the left to the right of the plots.

3.2.1 SFR versus z and M_*

Fig. 5 (top panels) presents the average log SFR versus the three different environments (field, filament, cluster) as a function of redshift (left) and M_* (right). The bottom panels of Fig. 5 show the average log SFR versus the three different galaxy types (isolated, satellite, central) as a function of redshift (left) and M_* (right). Overall, Fig. 5 confirms that the SFR is declining with cosmic time, consistent with the literature and the known fact that the SFR peaks at $z \sim 2$ (see Madau & Dickinson 2014; Sobral et al. 2014).

In the top-left panel of Fig. 5, at the lower redshift bin ($0.10 \leq z < 0.47$) we tentatively note a reduced SFR with increasing
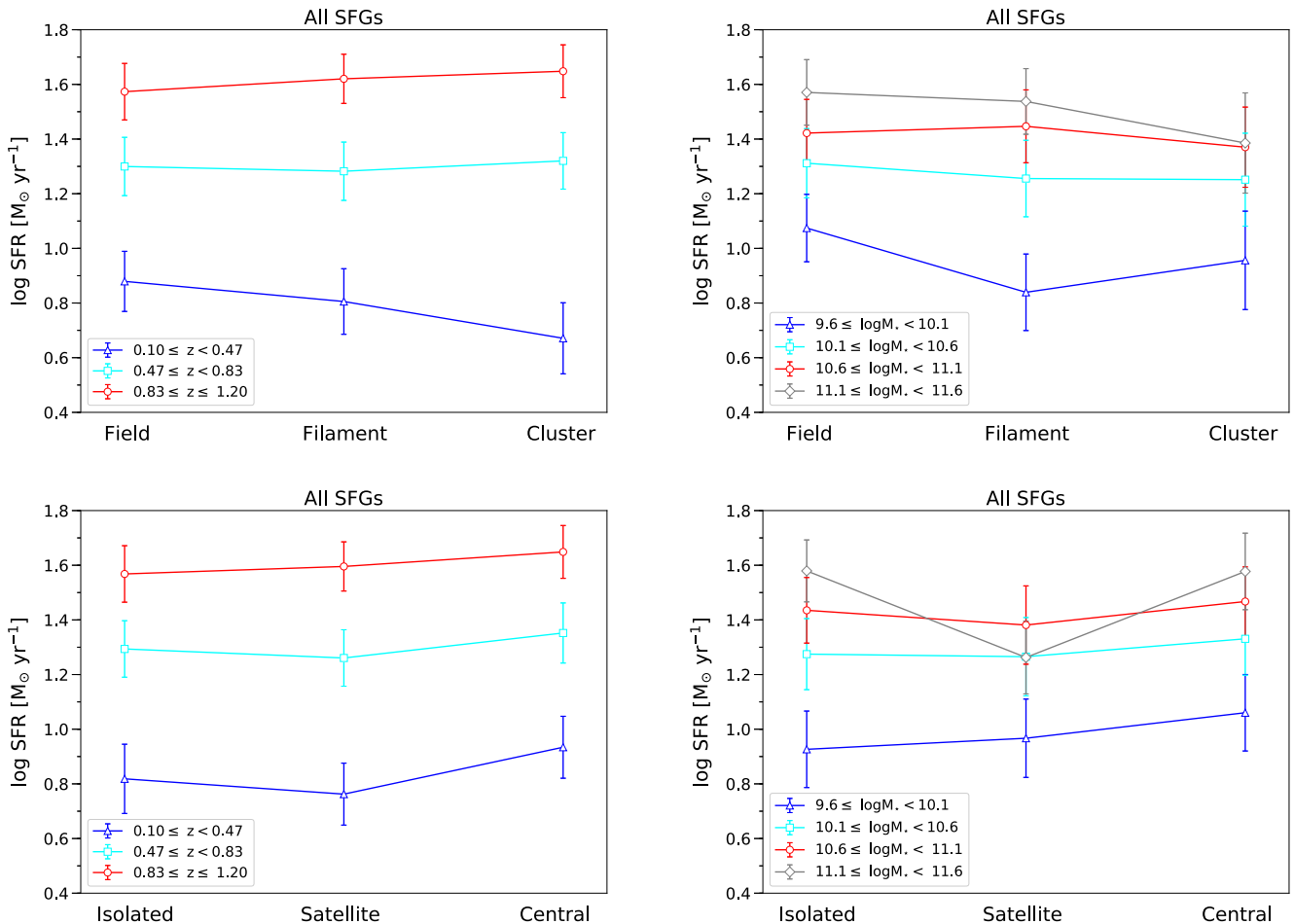

Figure 5. Top panels: SFR versus the three different environments (field, filament, cluster) as a function of redshift bin (left) and M_* bin (right). Bottom panels: SFR versus the three different galaxy types (satellite, central, isolated) as a function of redshift bin (left) and M_* bin (right). Error bars correspond to average 1σ errors based on the standard error of the mean. (A colour version of this figure is available in the online journal.)
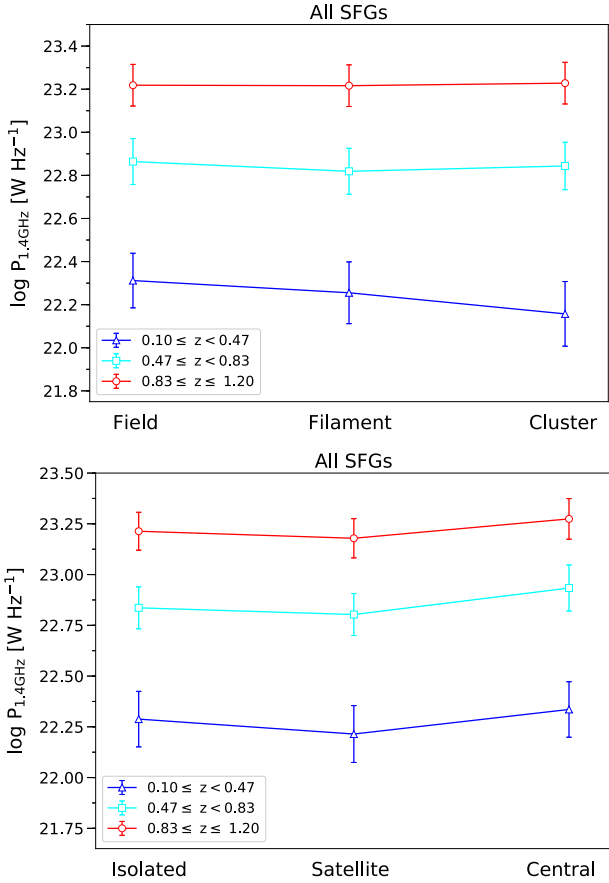
Figure 6. Averaged radio luminosity ($P_{1.4\,\mathrm{GHz}}$) versus the three different (field, filament, cluster) environments (top) and the three different galaxy (satellite, central, isolated) types (bottom) as a function of redshift bin. Error bars correspond to average 1σ errors based on the standard error of the mean. (A colour version of this figure is available in the online journal.)

environment density (i.e. from field, filament, to cluster). However, at the intermediate and higher redshift bins ($0.47 \leq z < 0.83$ and $0.83 \leq z \leq 1.20$), we do not see any obvious trend in SFR of SFGs from field to cluster. In the top-right panel of Fig. 5, for the lowest M_* bin ($9.6 \leq \log M_* < 10.1$), we can see that there is a reduced SFR from field to filament, then likely a higher SFR from filament to cluster. We see no trend for the higher M_* bin ($10.1 \leq \log M_* < 10.6$) and a tentative trend that the log SFR might be getting lower from field to cluster for the two highest M_* bins ($10.6 \leq \log M_* < 11.1$ and $11.1 \leq \log M_* < 11.6$). In the local Universe, star formation is dominated by field galaxies at different environments, as can be seen in Fig. 5 (top-left panel) while at intermediate and higher redshifts, filament and cluster galaxies might be more efficient at forming stars. We note that, given the error bars, the average SFR of SFGs might depend on the environment, particularly at the lowest redshift and stellar mass bins ($0.10 \leq z < 0.47$, $9.6 \leq \log M_* < 10.1$), as in the top panel of Fig. 5 with a tentative reduced SFR from field to cluster, probably implying that the MS of SFGs could vary with environment (e.g. Erfanianfar et al. 2016).

The bottom-left panel of Fig. 5 might show evidence of a higher SFR from isolated to central at all redshift bins. In the bottom-right panel of Fig. 5, we perhaps find a trend where the SFR might be getting higher from isolated to central for the three lowest M_* bins while the highest M_* bin likely shows a lower SFR for the satellite

SFGs, compared with isolated and central SFGs. We would note that, given the error bars, the SFR trend could particularly be more prominent at the lowest redshift and stellar mass bins ($0.10 \leq z < 0.47$, $9.6 \leq \log M_* < 10.1$) where the possibility of a higher SFR from isolated to central can be seen in the bottom panel of Fig. 5.

3.2.2 $P_{1.4\,\mathrm{GHz}}$ versus z

In Fig. 6, we plot the average log $P_{1.4\,\mathrm{GHz}}$ against the three different environments (top panel) and the three different galaxy types (bottom panel) as a function of redshift bin. As can be seen in Fig. 6, given the errors associated with these points, we effectively see no change in log $P_{1.4\,\mathrm{GHz}}$ both from field-to-cluster galaxies (top panel) and from isolated-to-central galaxies (bottom panel).

3.3 Possible caveats

There are some possible caveats that include selection bias, sample size (e.g. averaging a small number of sources in some bins) and completeness.

We focus on investigating the completeness limit of our radio-selected sample by estimating the minimum SFR (i.e. SFR limits), accessible to the VLA survey. We calculated the SFR limits based on equation (4) of Delhaize et al. (2017) using the minimum radio luminosity for each redshift bin (i.e. the SFR that corresponds to the radio flux density limit).

The SFR limits are shown by the horizontal dotted lines in the left panels of Fig. 4 for two assumed spectral index ($\alpha = 0.7$ and $\alpha = 0.8$) of the SFG population. There is one outlier cluster galaxy at $0.10 \leq z < 0.47$ and one field galaxy at $0.47 \leq z < 0.83$ and quite a few of the sources at $0.83 \leq z \leq 1.20$. These radio sources detected under SFR limits, regardless of their environment, observed at the highest redshift bin (i.e. $0.83 \leq z \leq 1.20$) appear to be associated with the spectral index as the two lines seem to depend on the assumed spectral index α as well as cosmic time. The sensitivity limits deepen as the spectral index steepens when redshift increases, possibly implying that a steeper spectral index would be needed for high-redshift radio sources.

We acknowledge that there might be the possibility of contamination by AGNs as our sample might still have galaxies that are in transition from star-forming to passive, with lower SFR (e.g. Vulcani et al. 2010) but are still detected as SFGs (i.e. more massive objects and at higher redshift). We have taken advantage of the results of the multiple AGN diagnostics that excluded already them from our sample and note that looking at the spectra of individual galaxies may help, but this is beyond the scope of the paper.

4 DISCUSSION

In Fig. 4, our comparison to the best-fitting lines from the literature may indicate shallower slopes in all environments, noting that the lowest and highest stellar mass bins have a lower average number of sources, and large error bars. We have measured a gradual evolution of the slope of the MS of SFGs toward shallower values at higher redshift bins (see Fig. 4). We find shallower slopes in the range of [0.2, 0.36] and normalizations in the range of [0.53, 2.90] for our radio-selected sample, as shown in Table 3. Our results are in agreement with the estimated values from previous work by Chen et al. (2009), Dunne et al. (2009), Oliver et al. (2010) and Sobral et al. (2014), who measured the slopes and normalization values in the range of [0.13, 0.40] and [0.30, 3.41], respectively. The fact that

we have much flatter slopes of the MS compared with Speagle et al. (2014) and Whitaker et al. (2012) might be a result of the evolution of the completeness limits with redshift. Other possibilities could be the averaging of a small number of sources at higher mass; with relevance to this, we note that in the highest M_* bin (11.1 ≤ log M_* < 11.6) we have the lowest number of sources. Karim et al. (2011) and Wuyts et al. (2012) have also found hints of a similar trend for the slope to flatten toward $z = 1$ or high M_*.

The variation of the slope of the MS with mass can be understood as an interplay between galaxy quenching and a depletion of the galaxy cold gas reservoir as M_* increases (e.g. Pan, Zheng & Kong 2017). In this scenario, it is known that there is an increase with redshift of the fraction of cold molecular gas (see Tacconi et al. 2010; Genzel et al. 2015) and the amount of dust (e.g. Dunne et al. 2011) available for star formation, implying that the availability of more cool gas leads to more star formation, raising the average SFR in SFGs. It has been observed that the slope of the MS becomes flatter (Dunne et al. 2009; Oliver et al. 2010; Sobral et al. 2014) generally at the higher M_* end while the flatness seems to be a function of redshift, which corroborates with our findings.

Apart from M_* and redshift, which affect the slope and the shape of the MS, there are environmental and morphological effects that play significant roles at least for galaxies in the local Universe (e.g. Popesso et al. 2019). This is found to be a result of starvation of cold gas inflows in galaxies, which may be truncated by a hot halo as observed in the studies of local galaxies by Popesso et al. (2019), as observed in our lower z bin. Environmental effects such as mergers (Peng et al. 2010; Narayanan et al. 2010; Hayward et al. 2011; Alaghband-Zadeh et al. 2012; Guo et al. 2013; Contini et al. 2020) may also be observed at higher stellar mass and z, although we do not see any apparent trend in Fig. 4 and also the limited statistics because of the lower number of sources in the highest mass bin does not permit us to confirm this.

At fixed stellar mass, previous studies (Poggianti et al. 2008; Ziparo et al. 2014) have found that environmental trends seem to weaken at higher redshift. Our results might suggest a similar weakening of environmental trends between the lowest and intermediate redshifts. As shown in Fig. 4, the MS shows the same type of flattening in all environments, with large error bars. Similarly, in Fig. 5, we do not see any trends as our results look flat and again there are large error bars. Overall, we point out that compared with the MS of Whitaker et al. (2012) and Speagle et al. (2014), we find the MS in all redshift bins to be considerably flatter, irrespective of environment.

We acknowledge that the numbers of sources in each bin are different for both redshift and stellar mass, equally spaced of 0.26 dex for z and 0.5 dex for M_*, respectively. The three redshift bins have a fairly similar number of sources (a factor of ∼1.6 maximum difference) and numbers increase as a function of redshift. However, as presented in Table 2, the numbers of sources in the lowest and highest stellar mass bins are lower compared with the two intermediate bins (by a factor of ∼8). By averaging a smaller number of sources in these two bins (particularly low numbers in cluster and at higher stellar mass) might affect the results in these bins when compared with the other bins.

To further investigate the environmental effects, we examine how the radio luminosity of SFGs is affected by the environment and galaxy type, as shown in Fig. 6. In studies of the far-infrared/radio correlation by, for example, Reddy & Yun (2004) and Randria-mampandry et al. (2015), it is observed that cluster galaxies have enhanced radio luminosity (relative to far-infrared emission) and it is attributed to be due to the impact of cluster environments on SFGs

at intermediate redshift. To check this, we further investigate the environmental effects on the radio luminosity of SFGs. We did not find clear evidence of any trends on the radio luminosity across the environments and galaxy types at all redshift bins.

5 CONCLUSIONS

In this paper, we present a study of the relationship between SFR and stellar mass M_* of SFGs, and also the relationship between environment and radio luminosity ($P_{1.4\,GHz}$), to shed new light on their differences with respect to environment as a function of redshift.

We use the large sample of SFGs from the VLA-COSMOS 3-GHz catalogue (Smolčić et al. 2017b) in three different environments (field, filament, cluster) for various types (isolated, satellite, central) of galaxies (Darvish et al. 2015, 2017). We investigate, for the first time, the distribution of SFGs with respect to the MS consensus region from the literature via z and M_* bins, taking into account these galaxy environments and using radio observations.

We summarize our main results as follows.

(i) Our results confirm that the SFR is declining with cosmic time, consistent with the literature, which states that the SFR density peaks at $z \sim 2$ (see Madau & Dickinson 2014; Sobral et al. 2014).

(ii) We find that the slope of the MS for different z and M_* bins is shallower than both the MS consensus and the best-fitting line of Whitaker et al. (2012). We measured a gradual evolution of the slope of the MS of SFGs toward shallower values at higher redshift bins, irrespective of environment, which is in agreement with previous values found by Chen et al. (2009), Dunne et al. (2009), Oliver et al. (2010) and Sobral et al. (2014).

(iii) We do not see any trend in log SFR as a function of both the environment and galaxy type, as given the large error bars the results could be consistent with one another. Furthermore, we note that overall the environment does not seem to be the cause of the flattening of the MS at high stellar masses in our radio flux-limited sample.

(iv) We observe that log $P_{1.4\,GHz}$ is a function of redshift. We also do not see any trend in log $P_{1.4\,GHz}$ as a function of both the environment and galaxy type, as given the large error bars the results could be consistent with one another. As such, the link between radio luminosity and galaxy type, and similarly the environment, for these SFGs does not seem to depend on redshift.

Deeper radio continuum data from the MeerKAT International GHz Tiered Extragalactic Exploration (MIGHTEE; Jarvis et al. 2016; Taylor & Jarvis 2017) survey in the COSMOS field will enable us to study larger samples of these galaxies. Furthermore, an investigation of the evolution of low-mass cluster blue galaxies in the COSMOS field using the recently available data from MIGHTEE/MeerKAT, complemented with ancillary data, is the subject of our upcoming manuscript.

ESO programme ID 179.A-2005 and on data products produced by TERAPIX and the Cambridge Astronomy Survey Unit on behalf of the UltraVISTA consortium.

DATA AVAILABILITY

The data underlying this article are available in CDS via anonymous ftp, at https://doi.org/10.1051/0004-6361/201630223. The data sets were derived from sources in the public domain: Smolčić et al. (2017b) via http://jvla-cosmos.phy.hr/dr1/; Darvish et al. (2015, 2017) via https://irsa.ipac.caltech.edu/data/COSMOS/tables/environment/; Laigle et al. (2016) via ftp://ftp.iap.fr/pub/from_users/hjmcc/COSMOS2015/.

REFERENCES

Alaghband-Zadeh S. et al., 2012, MNRAS, 424, 2232
Baldry I. K., Balogh M. L., Bower R. G., Glazebrook K., Nichol R. C., Bamford S. P., Budavari T., 2006, MNRAS, 373, 469
Barro G. et al., 2017, ApJ, 840, 47
Bell E. F., 2003, ApJ, 586, 794
Bonzini M. et al., 2015, MNRAS, 453, 1079
Bouwens R. J. et al., 2012, ApJ, 754, 83
Brinchmann J., Ellis R. S., 2000, ApJ, 536, L77
Brinchmann J., Charlot S., White S. D. M., Tremonti C., Kauffmann G., Heckman T., Brinkmann J., 2004, MNRAS, 351, 1151
Bruzual G., Charlot S., 2003, MNRAS, 344, 1000
Chabrier G., 2003, PASP, 115, 763
Chen Y.-M., Wild V., Kauffmann G., Blaizot J., Davis M., Noeske K., Wang J-M., Willmer C., 2009, MNRAS, 393, 406
Condon J. J., 1992, ARA&A, 30, 575
Contini E., Gu Q., Ge X., Rhee J., Yi S. K., Kang X., 2020, ApJ, 889, 156
Daddi E. et al., 2007, ApJ, 670, 156
Daddi E. et al., 2009, ApJ, 694, 1517
Darvish B., Mobasher B., Sobral D., Scoville N., Aragon-Calvo M., 2015, ApJ, 805, 121
Darvish B., Mobasher B., Martin D. C., Sobral D., Scoville N., Stroe A., Hemmati S., Kartaltepe J., 2017, ApJ, 837, 16
Davé R., Finlator K., Oppenheimer B. D., Fardal M., Katz N., Kereš D., Weinberg D. H., 2010, MNRAS, 404, 1355
Davé R., Oppenheimer B. D., Finlator K., 2011, MNRAS, 415, 11
Delhaize J. et al., 2017, A&A, 602, A4
Duarte M., Mamon G. A., 2014, MNRAS, 440, 1763
Dunne L. et al., 2009, MNRAS, 394, 3
Dunne L. et al., 2011, MNRAS, 417, 1510
Elbaz D. et al., 2007, A&A, 468, 33
Erfanianfar G. et al., 2016, MNRAS, 455, 2839
Finlator K., Davé R., Papovich C., Hernquist L., 2006, ApJ, 639, 672
Genzel R. et al., 2015, ApJ, 800, 20
Guo K., Zheng X. Z., Fu H., 2013, ApJ, 778, 23
Haines C. P. et al., 2013, ApJ, 775, 126
Hayward C. C., Kereš D., Jonsson P., Narayanan D., Cox T. J., Hernquist L., 2011, ApJ, 743, 159
Heavens A., Panter B., Jimenez R., Dunlop J., 2004, Nature, 428, 625
Huchra J. P., Geller M. J., 1982, ApJ, 257, 423
Ilbert O. et al., 2015, A&A, 579, A2
Jarvis M. et al., 2016, Proc. MeerKAT Science: On the Pathway to the SKA (MeerKAT2016). Stellenbosch, South Africa, p. 6 (available online at https://pos.sissa.it/cgi-bin/reader/conf.cgi?confid=277)

Jian H-Y. et al., 2017, ApJ, 845, 74
Jian H-Y. et al., 2018, PASJ, 70, S23
Karim A. et al., 2011, ApJ, 730, 61
Kennicutt Robert C. J., 1998a, ARA&A, 36, 189
Kennicutt Robert C. J., 1998b, ApJ, 498, 541
Kennicutt R. C., Evans N. J., 2012, ARA&A, 50, 531
Kochiashvili I. et al., 2015, A&A, 580, A42
Laigle C. et al., 2016, ApJS, 224, 24
Leja J., van Dokkum P. G., Franx M., Whitaker K. E., 2015, ApJ, 798, 115
Lin L. et al., 2014, ApJ, 782, 33
Madau P., Dickinson M., 2014, ARA&A, 52, 415
Magdis G. E., Elbaz D., Daddi E., Morrison G. E., Dickinson M., Rigopoulou D., Gobat R., Hwang H. S., 2010, ApJ, 714, 1740
Murphy E. J. et al., 2011, ApJ, 737, 67
Muzzin A. et al., 2012, ApJ, 746, 188
Narayanan D., Hayward C. C., Cox T. J., Hernquist L., Jonsson P., Younger J. D., Groves B., 2010, MNRAS, 401, 1613
Noeske K. G. et al., 2007, ApJ, 660, L43
Oliver S. et al., 2010, MNRAS, 405, 2279
Pan Z., Zheng X., Kong X., 2017, ApJ, 834, 39
Pannella M. et al., 2009, ApJ, 698, L116
Pannella M. et al., 2015, ApJ, 807, 141
Pearson W. J. et al., 2018, A&A, 615, A146
Peng Y-j. et al., 2010, ApJ, 721, 193
Poggianti B. M. et al., 2008, ApJ, 684, 888
Popesso P. et al., 2019, MNRAS, 483, 3213
Randriamampandry S. M., Crawford S. M., Cress C. M., Hess K. M., Vaccari M., Wilcots E. M., Bershady M. A., Wirth G. D., 2015, MNRAS, 447, 168
Reddy N. A., Yun M. S., 2004, ApJ, 600, 695
Rodighiero G. et al., 2011, ApJ, 739, L40
Salim S. et al., 2007, ApJS, 173, 267
Salmon B. et al., 2015, ApJ, 799, 183
Scoville N. et al., 2007, ApJS, 172, 1
Smolčić V. et al., 2017a, A&A, 602, A1
Smolčić V. et al., 2017b, A&A, 602, A2
Sobral D., Best P. N., Smail I., Mobasher B., Stott J., Nisbet D., 2014, MNRAS, 437, 3516
Speagle J. S., Steinhardt C. L., Capak P. L., Silverman J. D., 2014, ApJS, 214, 15
Stark D. P., Schenker M. A., Ellis R., Robertson B., McLure R., Dunlop J., 2013, ApJ, 763, 129
Steinhardt C. L. et al., 2014, ApJ, 791, L25
Tacchella S., Dekel A., Carollo C. M., Ceverino D., DeGraf C., Lapiner S., Mandelker N., Primack Joel R., 2016, MNRAS, 457, 2790
Tacconi L. J. et al., 2010, Nature, 463, 781
Taylor A. R., Jarvis M., 2017, IOP Conference Series: Materials Science and Engineering, 198, 012014
Treu T., Ellis R. S., Liao T. X., van Dokkum P. G., 2005, ApJ, 622, L5
Vulcani B., Poggianti B. M., Finn R. A., Rudnick G., Desai V., Bamford S., 2010, ApJ, 710, L1
Whitaker K. E., van Dokkum P. G., Brammer G., Franx M., 2012, ApJ, 754, L29
Whitaker K. E. et al., 2014, ApJ, 795, 104
Wuyts S. et al., 2012, ApJ, 753, 114
Ziparo F. et al., 2014, MNRAS, 437, 458

This paper has been typeset from a TeX/LaTeX file prepared by the author.